

AbsPoseLifter: Absolute 3D Human Pose Lifting Network from a Single Noisy 2D Human Pose

Ju Yong Chang
 Kwangwoon University
 jychang@kw.ac.kr

Gyeongsik Moon
 Seoul National University
 mks0601@snu.ac.kr

Kyoung Mu Lee
 Seoul National University
 kyoungmu@snu.ac.kr

Abstract

This study presents a new network (*i.e.*, *AbsPoseLifter*) that lifts a 2D human pose to an absolute 3D pose in a camera coordinate system. The proposed network estimates the absolute 3D location of a target subject and also outputs a considerably improved 3D relative pose estimation compared with those of existing pose lifting methods. We also propose using our *AbsPoseLifter* with a 2D pose estimator in a cascade fashion to estimate 3D human pose from a single RGB image. In this case, we empirically prove that using realistic 2D poses synthesized with the real error distribution of 2D body joints considerably improves the performance of our *AbsPoseLifter*. The proposed method is applied to public datasets to achieve state-of-the-art 2D-to-3D pose lifting and 3D human pose estimation.

1. Introduction

What information can we acquire from the sparse semantic points of a single image? Figure 1(a) shows a 2D human pose that consists of a set of 2D joints. Human activities can be easily recognized from such sparse 2D joint information [15], and automated algorithms [4, 14] based on such information have been proposed. What about the 3D human pose shown in Figure 1(b)? How accurately can 3D human pose (*i.e.*, 3D joint coordinates) be reconstructed using only projected geometric information without appearance features? This ill-posed problem [17], namely, the automatic lifting of 2D joint coordinates in a single image to 3D space, has been addressed in previous studies and successful methods have been proposed [21, 30]. However, existing methods output only the *relative 3D pose*, *i.e.*, the 3D joint coordinates after the translation transform is applied to move the reference joint to the origin. To address this issue, in this work, we propose a novel 2D-to-3D pose lifting network (*i.e.*, *AbsPoseLifter*) that can produce an *absolute 3D pose* in which the coordinates of all joints are defined on a camera coordinate system.

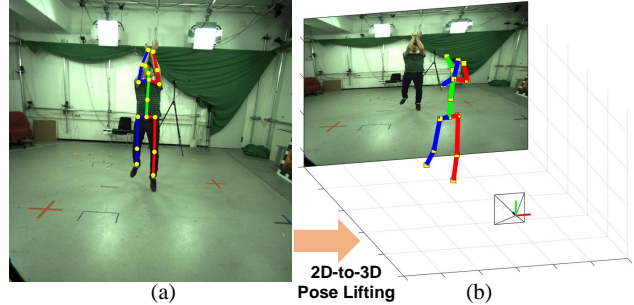


Figure 1: (a) A 2D human pose consisting of a set of several joints is overlaid on a RGB image. (b) Our goal is to estimate the 3D human pose in the camera coordinate system from such sparse 2D joint information in (a).

An absolute pose can be decomposed into the absolute coordinates of a reference joint (*i.e.*, the root) and the relative pose to it. In this work, to obtain an absolute 3D pose, we use the normalized 2D pose, 2D location, and 2D scale obtained by decomposing the input 2D pose. Among this 2D information, location and scale enable calculation of the root’s 3D coordinates. Specifically, location and scale provide information about the (X , Y) and Z (*i.e.*, depth) coordinates of the target human subject in the camera coordinates system, respectively. And, like the existing methods [21], the normalized 2D pose can be used for estimation of the root-relative 3D pose.

These two problems (*i.e.*, estimation of the root coordinates and relative 3D pose) should be dealt with together rather than independently, in which case a synergistic effect occurs. First, under perspective projection, the distance from the camera to the human subject (*i.e.*, root depth) is proportional to the ratio of the human scale in real space to the scale in the 2D image. The real scale can vary greatly depending on the posture of the human subject. For example, the scale in the squatting posture is relatively small compared to the stretching posture. This variation makes it difficult to determine the depth from only the 2D scale. However, if a root-relative 3D pose is available, this pro-

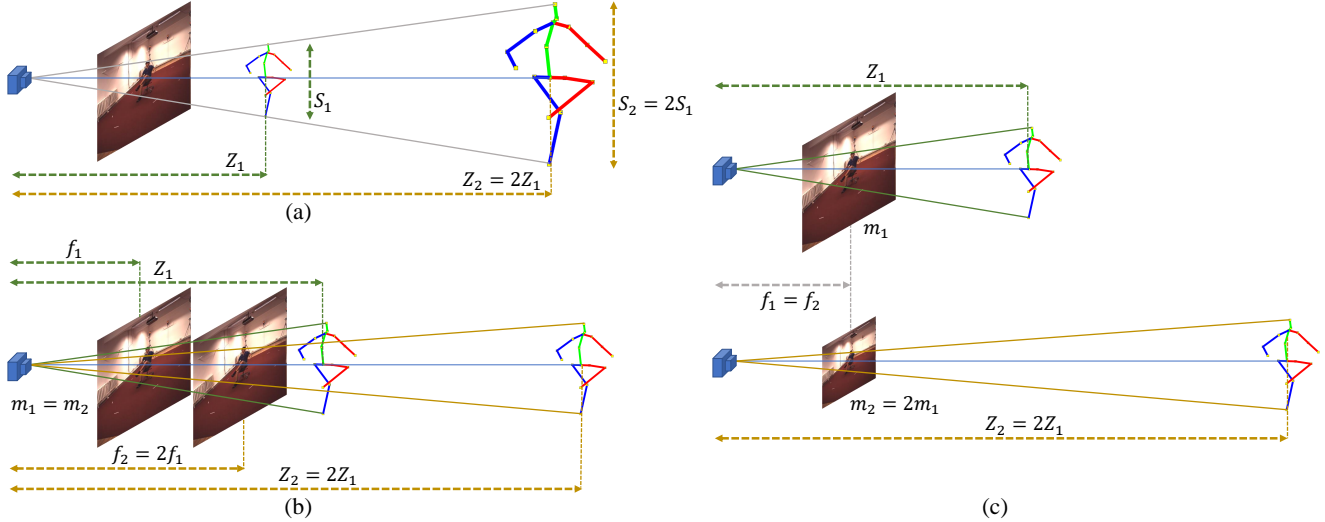


Figure 2: For a given input RGB image, the root’s absolute depth is proportional to the size of the human subject, as shown in (a). Even if the size of the human subject is fixed, the ambiguity in determining the absolute root depth remains due to the focal length. The focal length in terms of pixel dimensions (α) is the product of the focal length in terms of physical dimensions (f) and the number of pixels per unit distance (m): $\alpha = f \times m$. Under the assumption of fixed subject size, the absolute root depth corresponding to a given input RGB image is proportional to f and m , shown in (b) and (c), respectively. Note that when m is doubled ($m_2 = 2m_1$), the actual physical size occupied by the image in the image sensor is halved, which doubles the absolute root depth ($Z_2 = 2Z_1$).

vides additional information about the real scale, helping to calculate the depth of the root accurately.

Determination of the root-relative 3D pose can also be aided by the root’s 3D location information. It is because this additional information can alleviate the ill-posedness of the problem. For example, under the perspective projection assumption, a single projected 2D pose can correspond to multiple root-relative 3D poses unless the root’s absolute coordinates are not provided. This causes ambiguities in estimating the correct root-relative 3D pose from a given 2D pose. However, given the information of absolute root coordinates, these ambiguities can be easily resolved. Therefore, in this work, we propose a method for *estimating the root coordinates and root-relative 3D pose simultaneously*.

In fact, of our two goals, determining the absolute depth of the root is a significantly unconstrained problem. Technically, the ambiguities of the human subject size and camera focal length do not allow the absolute depth of the root to be uniquely determined, which is illustrated in Figure 2. This problem is solved in this study as follows. First, in the proposed AbsPoseLifter, the size of the human subject is learned implicitly from datasets, which resolves the *size ambiguity*. Also, to handle the *focal length ambiguity*, AbsPoseLifter outputs the *canonical root depth* normalized by the focal length instead of the real depth. If additional focal length information is available, we can obtain the root’s real depth from the canonical depth.

The proposed AbsPoseLifter can be applied to estimate the absolute 3D pose of a person from a single 2D image. A simple approach to achieve this goal is to combine a 2D human pose estimator and the AbsPoseLifter sequentially. That is, the 2D human pose estimator generates a 2D pose from the input 2D image, and the resulting 2D pose is fed into AbsPoseLifter to output the corresponding absolute 3D pose. However, commonly, the results of 2D pose estimation are unreliable due to inevitable errors. A recent study [31] indicates that such errors exhibit a similar distribution regardless of the type of 2D pose estimator used, and a method for improving the performance of existing 2D pose estimators by utilizing such distribution is proposed [24]. In this regard, we propose to analyze the error of a 2D pose estimator and synthesize the input of AbsPoseLifter for learning following the resulting error statistics.

In summary, we propose the following significant technical improvements to 3D human pose estimation.

- The first is implemented in the *normalization layer*, which is the first layer of the proposed AbsPoseLifter. Our novel normalization layer normalizes the input 2D pose and adds the target subject’s 2D location and scale information as intermediate features. These added features not only enable the estimation of the root’s absolute 3D coordinates but also considerably improve the performance of root-relative 3D pose estimation.

- The second is the *canonical loss function* that causes the AbsPoseLifter to produce a canonical root depth that is independent of the camera focal length. This new loss function allows the AbsPoseLifter to be applied to any test image with an unknown focal length.
- The last one focuses on the *connection between 2D pose estimation and 3D pose lifting modules*. In our method, the error of a 2D pose estimator is realistically synthesized, and the result is used to learn the 3D pose lifter, thereby making our AbsPoseLifter robust to 2D pose estimation errors. Consequently, the proposed approach achieves the state-of-the-art performance on two large-scale 3D human pose datasets, namely, Human3.6M [13] and MPI-INF-3DHP [22].

The remainder of this paper is organized as follows. Section 2 introduces related studies. Section 3 describes the proposed 2D-to-3D pose lifting method (*i.e.*, AbsPoseLifter). Section 4 explains the application of this method to 3D human pose estimation from a single RGB image. Section 5 presents the experimental results. Section 6 provides the conclusions drawn from the study.

2. Related work

2.1. 2D-to-3D human pose lifting

In earlier studies, 3D human pose is typically modeled as a linear combination of sparse basis poses. In general, the re-projection error between the 2D projections of 3D joints and input 2D joints is minimized by using optimization methods, such as greedy orthogonal matching pursuit [30], alternating direction [40], and convex relaxation-based alternating direction method of multipliers [44], along with a prior model of physically possible 3d poses [1]. After optimization, the 3D joints in a world coordinate system and the viewpoint information of an orthographic camera are obtained simultaneously.

In recent studies, a large 2D/3D dataset is used to learn a regression function that directly converts the input 2D pose to the output 3D pose based on a camera coordinate system. A neural network is typically adopted for this purpose, and normalized 2D joint coordinates [21] and a Euclidean distance matrix [25] are proposed as inputs for the network. All the aforementioned methods yield a relative pose based on the root, whereas our proposed method allows the acquisition of an absolute 3D pose.

2.2. 3D human pose estimation from a single image

Recent deep learning-based methods can be divided into direct image-to-pose estimation and cascade approaches. The *direct approach* produces an output 3D pose directly from an input single RGB image. Such outputs exhibit various forms, such as 3D joint coordinates [18], bone-based

representations [35], and volumetric heatmaps [29]. Recent studies [33] and [36] have proposed methods that directly regress 3D coordinates while maintaining the advantages of a volumetric heatmap representation through a soft-argmax [20, 27] operation. In particular, the method presented in [33] is related to our method, given that both approaches calculate the absolute 3D coordinates of the root. However, the previous method differs from our method, which uses only 2D joint information for pose lifting, whereas the method of [33] requires an RGB image as input. Absolute root coordinates were also computed in [22]. To do so, the method in [22] initially computes the root-relative pose using the network learned through transfer learning, and then estimates the absolute location of the root through a post-processing process based on a closed-form formula. In [33] and [22], only the evaluation of the root-relative pose is performed, whereas the performance of absolute root location estimation is not reported.

The *cascade approach* consists of two steps: (1) creating a 2D pose through a 2D pose estimator and (2) lifting this 2D pose to output a 3D pose. The acquisition of a 3D pose from a 2D pose is accomplished via neural network-based regression [8, 21, 25] or by fitting a 3D morphable model to 2D joints [3]. The cascade approach is flexible and easy to use thanks to its modular design. Besides, different types of datasets can be used for learning 2D pose estimating and 2D-to-3D pose lifting modules. On the other hand, in the direct approach, the entire process for generating an output 3D pose from an input RGB image is optimized in an end-to-end fashion by a single cost function, which is considered to bring relatively high performance. Our method is a regression-based cascade approach, which nevertheless achieves better 3D human pose estimation performance than most existing direct approaches.

2.3. Error analysis of 2D human pose estimation

In [31], prediction errors in 2D human pose estimation were categorized into various types, thereby experimentally proving that existing state-of-the-art methods produce similar error distributions. On the basis of taxonomy, a joint with a small error from ground truth is considered *good*. The error of a joint that is near the ground truth but is larger, is called a *jitter*. *Inversion* and *swap* represent errors due to confusion with semantically similar joints belonging to the same and different persons, respectively. Lastly, a *miss* corresponds to a considerably large error that does not belong to the previous cases. The method proposed in [24] refines the prediction results of existing 2D pose estimators by using estimation error statistics. In contrast with this previous study that uses a simple empirical ratio of error types, our method estimates a specific error distribution to make 3D pose lifting robust.

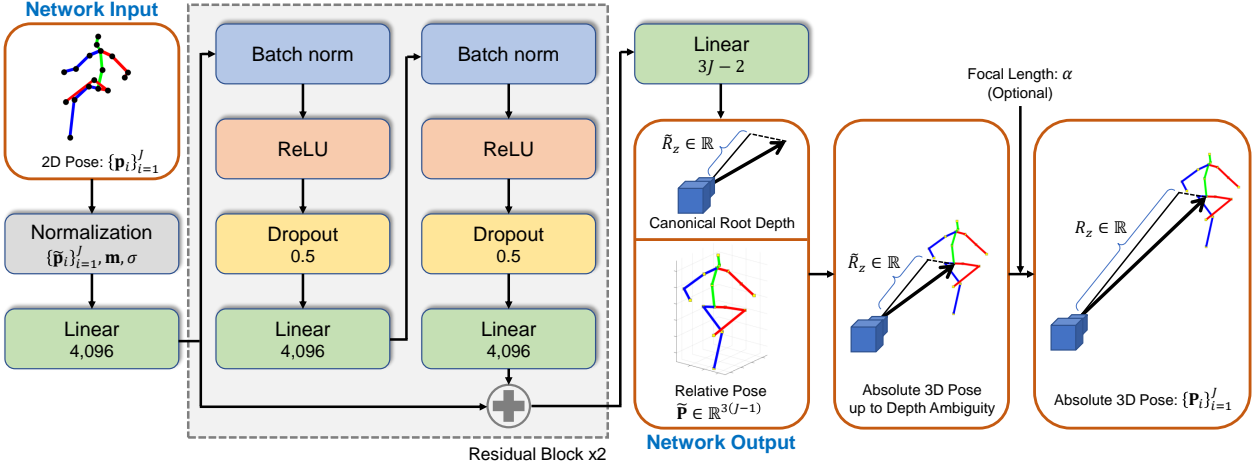


Figure 3: Structure of the proposed AbsPoseLifter.

3. AbsPoseLifter

3.1. Input and output for AbsPoseLifter

The objective of the pose lifting problem is to lift a given 2D pose $\{\mathbf{p}_i\}_{i=1}^J$ to a 3D pose $\{\mathbf{P}_i\}_{i=1}^J$. $\mathbf{p}_i \in \mathbb{R}^2$ and $\mathbf{P}_i \in \mathbb{R}^3$ represent the locations of the i th joint in an input image coordinate system and a camera coordinate system, respectively; and J denotes the number of joints. First, we apply the two-step normalization procedure to the input 2D pose. In the first step, we convert 2D coordinates $\mathbf{p}_i = [x_i, y_i]$ to $\mathbf{p}'_i = [x'_i, y'_i]$ for all joints i as follows:

$$\begin{aligned} x'_i &= x_i - c_x; \\ y'_i &= y_i - c_y, \end{aligned} \quad (1)$$

where (c_x, c_y) denotes the principal point of the camera. This transformation makes the coordinates of the 2D joint independent of the principal point of the camera. If the principal point of a test image is unknown, we can use the image center approximately. According to our experiments on Human3.6M and MPI-INF-3DHP, this approximation does not yield a quantitatively significant performance difference.

In the second step, we follow the previous pose lifting methods [21] and further normalize the input 2D joints to zero mean and unit variance as follows:

$$\tilde{\mathbf{p}}_i = \frac{(\mathbf{p}'_i - \mathbf{m})}{\sigma}, \quad (2)$$

where \mathbf{m} and σ denote the mean vector and standard deviation, respectively:

$$\mathbf{m} = \sum_{i=1}^J \mathbf{p}'_i / J, \quad (3)$$

$$\sigma = \sqrt{\sum_{i=1}^J \|\mathbf{p}'_i - \mathbf{m}\|^2 / J}. \quad (4)$$

Note that \mathbf{m} and σ represent the approximated 2D *location* and *scale* of the subject in the image, respectively. Under a perspective projection assumption, this 2D location and scale information provides a clue to the 3D location of the subject, and allows the estimation of an absolute 3D pose. Therefore, we define a normalization layer that transforms the input $(2J)$ -dimensional vector $\mathbf{p} = [\mathbf{p}_1, \dots, \mathbf{p}_J]$ into a $(2J+3)$ -dimensional vector concatenated with normalized 2D coordinates, mean vector, and standard deviation. We then set this layer as the first layer of our AbsPoseLifter. Notably, the method of [21] does not perform normalization by the principal point and does not use information about the location and scale of the target subject.

Our objective in pose lifting is to obtain an absolute 3D pose $\{\mathbf{P}_i\}_{i=1}^J$. It can be decomposed into the root's absolute coordinates $\mathbf{R} = [R_x, R_y, R_z] \in \mathbb{R}^3$, and the relative 3D pose $\{\tilde{\mathbf{P}}_i\}_{i=1}^J$ to the root: $\mathbf{P}_i = \mathbf{R} + \tilde{\mathbf{P}}_i$. We estimate $\tilde{R}_z = \frac{R_z}{\alpha}$ obtained by dividing the z -component R_z of the root by the focal length α instead of its absolute 3D coordinates. \tilde{R}_z means a depth value that is independent of the focal length of the camera, so it is named *canonical root depth* in this study. Therefore, 2D-to-3D pose lifting can be formulated as the problem of finding a 3D *regression function* $h : \mathbb{R}^{2J} \rightarrow \mathbb{R}^{3J-2}$ that maps the input 2D pose $\mathbf{p} \in \mathbb{R}^{2J}$ into the canonical root depth $\tilde{R}_z \in \mathbb{R}$ and the root-relative 3D pose $\tilde{\mathbf{P}} \in \mathbb{R}^{3J-3}$.

From the canonical depth \tilde{R}_z and the root's 2D coordinates $\mathbf{r} = [r_x, r_y]$, the x , y -components R_x and R_y of the absolute root coordinates are obtained by the reprojection formula as follows:

$$\begin{aligned} R_x &= (r_x - c_x) \frac{R_z}{\alpha} = (r_x - c_x) \tilde{R}_z; \\ R_y &= (r_y - c_y) \frac{R_z}{\alpha} = (r_y - c_y) \tilde{R}_z. \end{aligned} \quad (5)$$

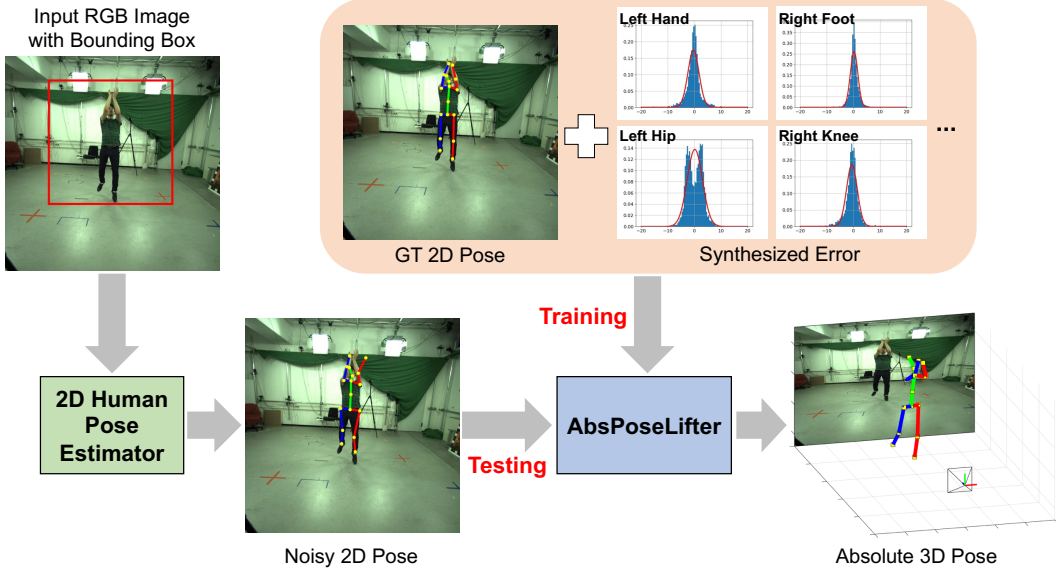


Figure 4: Overview of the proposed 3D human pose estimation method from a single RGB image.

Note that root's absolute x and y -coordinates can be calculated without focal length information. Meanwhile, the absolute root depth R_z is obtained as follows:

$$R_z = \alpha \tilde{R}_z. \quad (6)$$

Therefore, for any test image, we can reconstruct up to the canonical root depth \tilde{R}_z , which can be promoted to the absolute root depth R_z with the help of focal length information.

3.2. Network structure

We describe the structure of our AbsPoseLifter that realizes the 3D regression function h , which is shown in Figure 3. Our network is primarily based on the residual block proposed in [21]. This block iteratively passes the input vector to batch normalization [12], dropout [34], the rectified linear unit [26], and linear layers twice, and then adds the result to the residual connection [11] output. The dropout probability and feature dimension are set to 0.5 and 4096, respectively.

First, the input $(2J)$ -dimensional vector is normalized to a $(2J + 3)$ -dimensional vector via the normalization layer. The latter is then converted to a 4096-dimensional feature vector through a linear layer. This vector passes through two residual blocks and finally outputs a $(3J - 2)$ -dimensional vector via a linear layer. The first number represents the canonical root depth \tilde{R}_z , whereas the following $3(J - 1)$ numbers represent the root-relative pose vector $\tilde{\mathbf{P}}$, except for the root.

Subsequently, we supervise our AbsPoseLifter using the ground truth root depth R_z^* , focal length α , and relative pose

$\tilde{\mathbf{P}}^*$ for learning the 3D regression function h . In particular, the following cost function based on L1 loss is minimized:

$$L = \frac{1}{N} \sum_{i=1}^N |\tilde{R}_z^{(i)} - \frac{R_z^{*(i)}}{\alpha}| + \lambda \frac{1}{N} \sum_{i=1}^N \|\tilde{\mathbf{P}}^{(i)} - \tilde{\mathbf{P}}^{*(i)}\|_1, \quad (7)$$

where superscript i is the index of the sample, and N denotes the total number of training samples. We call the first term a *canonical loss function* because it causes our network to output a canonical root depth that is independent of the focal length. λ is a parameter for adjusting the relative strength between the two loss functions for the canonical root depth and the root-relative pose. It is set to 10^3 in all our experiments.

4. Cascading with 2D pose estimator

An absolute 3D pose can be obtained from a single RGB image using the AbsPoseLifter presented in the previous section. The basic concept is to combine a state-of-the-art 2D human pose estimation method and AbsPoseLifter in a cascade fashion, as shown in Figure 4. Similar to other 3D human pose estimation studies, we assume that a single RGB image and a bounding box that contains the target subject in the image are provided as inputs. First, we crop the input image using the bounding box and then resize the resulting image to 256×256 . We then feed the resized image into a state-of-the-art 2D human pose estimator to obtain a 2D pose. Thereafter, the obtained 2D pose is transformed into the original image's coordinate system and fed into our AbsPoseLifter to yield the canonical root depth \tilde{R}_z and the root-relative pose $\tilde{\mathbf{P}}$. If focal length information is

available, the canonical root depth can be converted to the absolute root coordinates $\mathbf{R} = (R_x, R_y, R_z)$ through Equations (5) and (6), and finally, the absolute root coordinates and the root-relative pose are transformed into an absolute 3D pose using $\mathbf{P}_i = \mathbf{R} + \tilde{\mathbf{P}}_i$.

4.1. 2D human pose estimation

For 2D human pose estimation from a single RGB image, we use the recently proposed heatmap regression network [41] and integral regression [36]. The method presented in [41] removes the last two layers of a residual neural network (*i.e.*, ResNet) [11] and adds three deconvolution layers and a 1×1 convolution layer to the back. This modified network receives an image with a size of $3 \times 256 \times 256$ and generates output heatmaps with a size of $J \times 64 \times 64$, which intuitively represent probability distributions for the 2D locations of each joint.

The process of obtaining 2D joint coordinates from heatmaps generally depends on the argmax operation, which has two drawbacks: (1) it is vulnerable to quantization errors and (2) it is nondifferentiable. Therefore, a method that can directly calculate the 2D joint coordinates from a heatmap with sub-pixel accuracy in a differentiable manner has been proposed for integral regression [36]. The basic concept of this method is to normalize a heatmap to a probability distribution and then apply the expectation operation to the result.

In this study, we construct a 2D human pose estimator by attaching an integral module to the back of the heatmap regression network based on the ResNet backbone. This estimator outputs the heatmaps and 2D joint coordinates from an input RGB image. The mean squared error (MSE) and L1 losses are used to supervise the heatmaps and 2D coordinates, respectively, as a cost function for estimator learning.

4.2. Synthesizing the input for training AbsPoseLifter

The result of the 2D pose estimator is used as the input for our AbsPoseLifter to generate an absolute 3D pose. Such input 2D pose is imperfect and includes an estimation error. We propose to model the estimation error and use the sampled realistic 2D pose based on the error distribution for the learning of AbsPoseLifter to make it robust to error.

To obtain the error statistics of 2D pose estimation, we learn a 2D human pose estimator using data, excluding one of the human subjects that constitute the training set. The estimation error is obtained by applying the learned model to the excluded human subject data, as shown in Figure 5. We propose that a simple mixture model consisting of Gaussian and uniform distributions is well suited for such an empirical error distribution. Following the error taxonomy in [31], the Gaussian and uniform distributions seem to account for the error of the inlier joint, such as *good* or *jitter*,

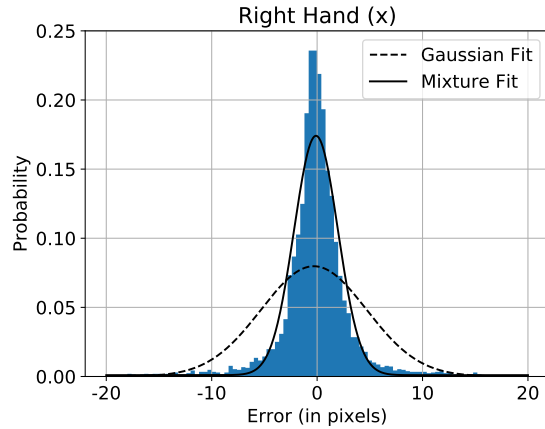


Figure 5: The error distribution of the *right hand* joint in the *x* axis is shown in the blue histogram. The dotted and solid lines show the single Gaussian model and the proposed mixture model fitted to such empirical data, respectively.

and the error of the outlier joint, such as *inversion* or *miss*, respectively.

The mixture model for error $\mathbf{e} = (e_x, e_y)$ is as follows:

$$p(\mathbf{e}) = \gamma \frac{\exp\left(-\frac{1}{2}(\mathbf{e} - \boldsymbol{\mu})^T \boldsymbol{\Sigma}^{-1}(\mathbf{e} - \boldsymbol{\mu})\right)}{2\pi\sqrt{|\boldsymbol{\Sigma}|}} + (1-\gamma) \frac{1}{v}, \quad (8)$$

where γ is the mixing parameter; v is the normalization constant of the uniform distribution; and $\boldsymbol{\mu} = (\mu_x, \mu_y)$ and $\boldsymbol{\Sigma} = \text{diag}(\sigma_x^2, \sigma_y^2)$ represent the mean vector and covariance matrix of the Gaussian distribution, respectively. We initially set v to $100 \times 100 = 10000$, assuming that the pixel range of the error due to the outlier is $[-50, 50]$. The remaining parameters of the mixture model are determined by minimizing the negative log likelihood as follows:

$$NLL = - \sum_i \log p(\mathbf{e}^{(i)}), \quad (9)$$

where superscript i is the index of the sample. This minimization process can be realized using the expectation maximization (EM) algorithm [6].

To estimate the parameters using the EM algorithm, we introduce a latent variable $z^{(i)} \in \{0, 1\}$ that determines from which the i th sample with an error vector $\mathbf{e}^{(i)}$ comes. $z^{(i)} = 0$ and $z^{(i)} = 1$ indicate that the sample originates from a uniform distribution and a single Gaussian distribution, respectively. The EM algorithm consists of two steps: (1) compute the expectation of $z^{(i)}$ using the current estimate of parameters, and (2) compute new model parameters using the estimate of $z^{(i)}$. This procedure is repeated until convergence to estimate the model parameters, which typically requires two or three iterations. The detailed procedure of the EM algorithm is summarized in Al-

Algorithm 1: EM algorithm for estimating the parameters or our error model

Input: error vectors $\{\mathbf{e}^{(i)}\}_{i=1}^N$

- 1 Initialize model parameters $\Theta = (\boldsymbol{\mu}, \boldsymbol{\Sigma}, \gamma)$
- 2 **while** not converged **do**
- 3 **(E-Step)** Compute membership probabilities
- 4 **for** $i = 1, \dots, N$ **do**
- 5 $p_0^{(i)} \leftarrow \frac{1}{v}$
- 6 $p_1^{(i)} \leftarrow \frac{\exp\left(-\frac{1}{2}(\mathbf{e}^{(i)} - \boldsymbol{\mu})^T \boldsymbol{\Sigma}^{-1}(\mathbf{e}^{(i)} - \boldsymbol{\mu})\right)}{2\pi\sqrt{|\boldsymbol{\Sigma}|}}$
- 7 $\eta_0^{(i)} \leftarrow \frac{\gamma p_0^{(i)}}{(1-\gamma)p_0^{(i)} + \gamma p_1^{(i)}}$
- 8 $\eta_1^{(i)} \leftarrow \frac{\gamma p_1^{(i)}}{(1-\gamma)p_0^{(i)} + \gamma p_1^{(i)}}$
- 9 **(M-Step)** Maximize expected log-likelihood
- 10 $\boldsymbol{\mu} \leftarrow \frac{\sum_{i=1}^N \eta_1^{(i)} \mathbf{e}^{(i)}}{\sum_{i=1}^N \eta_1^{(i)}}$
- 11 $\boldsymbol{\Sigma} \leftarrow \frac{\sum_{i=1}^N \eta_1^{(i)} (\mathbf{e}^{(i)} - \boldsymbol{\mu})(\mathbf{e}^{(i)} - \boldsymbol{\mu})^T}{\sum_{i=1}^N \eta_1^{(i)}}$
- 12 $\gamma \leftarrow \frac{\sum_{i=1}^N \eta_1^{(i)}}{\sum_{i=1}^N (\eta_0^{(i)} + \eta_1^{(i)})}$

Output: model parameters $\Theta = (\boldsymbol{\mu}, \boldsymbol{\Sigma}, \gamma)$

gorithm 1, in which $\eta_0^{(i)}$ and $\eta_1^{(i)}$ denote membership probabilities $\Pr(z^{(i)} = 0 | \mathbf{e}^{(i)}; \Theta)$ and $\Pr(z^{(i)} = 1 | \mathbf{e}^{(i)}; \Theta)$, respectively.

To obtain the initial estimate of the mean and covariance of the Gaussian distribution, a single Gaussian is fitted to the given error data, and γ is initialized to 0.9. Figure 5 shows that our mixture model effectively explains the empirical error data. The error model obtained through the preceding procedure is used to synthesize the 2D input pose of the training set required for AbsPoseLifter learning, thereby making the resulting AbsPoseLifter robust to real 2D pose estimation error.

5. Experimental results

5.1. Implementation details

PyTorch [28] is used as the deep learning framework in all our experiments. AbsPoseLifter and the 2D pose estimator are learned separately through the following processes.

AbsPoseLifter. First, the cost function of Equation (7) is minimized using the Rmsprop optimization algorithm [37] for AbsPoseLifter learning. Learning rate, batch size, and number of epochs are set to $1e^{-3}$, 64, and 300, respectively. Learning rate is reduced to $1e^{-4}$ after 200 epochs. Except for random horizontal flipping, no data augmentation is performed in 2D-to-3D pose lifting experiments. In the case of 3D human pose estimation from a single RGB image, the input synthesis process in Section 4.2 functions as an additional data augmentation procedure.

2D pose estimator. The ResNet152 backbone-based network for 2D pose estimation is initialized with pre-trained weights from the ImageNet dataset [32]. Then, the sum of the MSE heatmap and L1 coordinate losses in Section 4.1 is minimized using the Rmsprop algorithm. In this case, learning rate, batch size, and number of epochs are set to $1e^{-4}$, 48, and 60, respectively. Learning rate is reduced to $1e^{-5}$ after 30 epochs. For data augmentation, a small random translation of $[-4, 4]$ pixel range, random horizontal flipping, and 40% random color jittering are applied to the input RGB image.

5.2. Dataset and evaluation metrics

The datasets and metrics used to evaluate the performance of the proposed method are as follows.

Human3.6M. Human3.6M dataset [13] is used as the primary dataset for evaluating the proposed method. This dataset consists of approximately 3.6M RGB images and their corresponding 2D and 3D poses obtained from 11 actors performing 15 activities using a motion capture system that includes 4 cameras. In addition, we use the MPII dataset [2] for the learning of the 2D pose estimator. This dataset consists of approximately 25K in-the-wild images and their corresponding 2D pose information.

For the evaluation metric, we use the mean per joint position error (MPJPE), which is defined as the mean of the Euclidean distances between the corresponding joints after aligning the root joints of ground truth 3D pose and the estimated 3D pose. Moreover, the PA-MPJPE, which is calculated after applying Procrustes alignment [9] to the two 3D poses, is adopted as an additional metric. The two metrics are used to evaluate the root-relative pose computed using our method. To evaluate the absolute location of the root joint, we introduce the mean of the Euclidean distance between the prediction \mathbf{R} and the ground truth \mathbf{R}^* , i.e., the mean of the root position error (MRPE), as a new metric:

$$MRPE = \frac{1}{N} \sum_{i=1}^N \|\mathbf{R}^{(i)} - \mathbf{R}^{(i)*}\|_2, \quad (10)$$

where superscript i is the index of the sample, and N denotes the total number of test samples.

We use two protocols adopted from existing works to evaluate the proposed method. In *Protocol 1*, Subjects 1, 5, 6, 7, 8 and Subjects 9, 11 are used as the training and test sets, respectively. Evaluation is performed through the MPJPE metric. In *Protocol 2*, Subjects 1, 5, 6, 7, 8, 9 and Subject 11 are adopted as the training and test sets, respectively. The PA-MPJPE metric is used for evaluation.

MPI-INF-3DHP. To evaluate the proposed method, we also use the MPI-INF-3DHP dataset [22]. This dataset consists of approximately 1.3M frames acquired using a commercial marker-less motion capture system with multiple

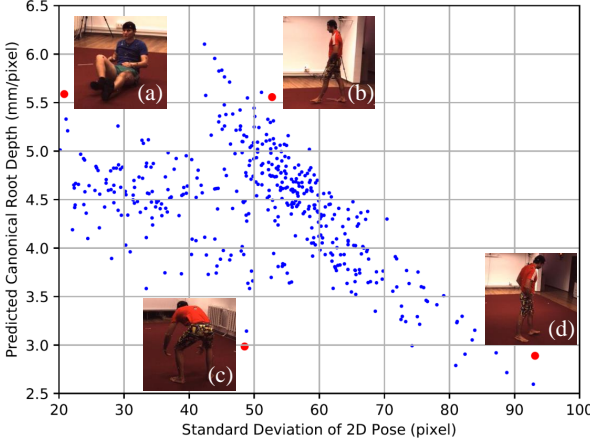


Figure 6: The standard deviation (σ) of the 2D pose of the test samples in the Human3.6M dataset and the canonical root depth (\tilde{R}_z) predicted by our AbsPoseLifter are plotted.

Method	MPJPE	PA-MPJPE	MRPE
Baseline	44.86	29.24	510.88
+ Location	39.04	29.09	368.89
+ Scale	44.29	28.90	113.38
+ Location & scale	38.38	28.78	98.84
Ramakrishna [30]	-	89.50	-
Dai [5]	-	72.98	-
Zhou [44]	-	50.04	-
Zhou [45]	-	49.64	-
Moreno-Noguer [25]	-	62.17	-
Martinez [21]	-	37.10	-

Table 1: 2D-to-3D pose lifting performances are shown for our AbsPoseLifter and its variants and other existing methods, in which the Human3.6M dataset is used. Protocol 1 is adopted and the unit of all numbers is mm .

cameras. Approximately 190K frames obtained by sampling the training set every 5 frames are used for the learning of the proposed model. Meanwhile, the original test set that consists of 2,935 frames is used for evaluation.

In addition, 3DPCK that extends the existing percentage of correct keypoints (PCK) [38, 39] to 3D and the area under curve (AUC) that is calculated for several PCK thresholds are used as evaluation metrics. To compute 3DPCK, whether the distance between the corresponding joints is less than 150mm is checked after aligning the roots of the predicted and ground truth 3D poses. The data acquisition environment for the test set can be divided into a studio with a green screen, a studio without a green screen, and outdoor. 3DPCK and AUC are reported for each case.

5.3. 2D-to-3D pose lifting

In this subsection, we present the performance of the proposed AbsPoseLifter for 2D-to-3D pose lifting.

Canonical root depth estimation. Under the perspective projection assumption, for human subjects with a constant real scale, the canonical root depth is inversely proportional to the image scale. This inverse proportion property is learned implicitly by the proposed AbsPoseLifter, as shown in Figure 6, where the predicted canonical root depth is approximately in inverse proportion to the human scale in image space (*i.e.*, the standard deviation of the 2D pose). However, the various postures of the human subject lead to variations in real scale, making it difficult to estimate the canonical root depth using only the inverse proportion property. This problem can be resolved by our method, which allows us to estimate the root-relative 3D pose and thus implicitly compute the variation of the real scale for a more accurate estimation of the canonical root depth. For example, for Figures 6(a) and (b) with different image scales, the proposed method estimates similar canonical root depths, taking into account variations in real scales.

Performance analysis. We first evaluate the performance of our AbsPoseLifter for 2D-to-3D pose lifting. To achieve this, we train and test our AbsPoseLifter using ground truth 2D pose data. Table 1 presents the performance of our AbsPoseLifter with and without location and scale information. To implement the latter, we modify our normalization layer to output only normalized 2D pose $\{\tilde{\mathbf{p}}_i\}_{i=1}^J$, except for mean \mathbf{m} and standard deviation σ . The experimental results indicate that using location and scale information is very important in estimating an accurate absolute root position. In this case, MRPE is 98.84mm. Moreover, the location and scale information required for absolute root estimation considerably reduces the root-relative pose error (MPJPE) from 44.86mm to 38.38mm. This result demonstrates the effectiveness of our proposed AbsPoseLifter in estimating the absolute pose (*i.e.*, the absolute root coordinates and the root-relative pose).

Quantitative comparison. Subsequently, we perform a quantitative comparison between the proposed method and existing methods for 2D-to-3D pose lifting. The results are provided in Table 1. The proposed method outperforms optimization-based methods [5, 30, 44, 45] and the more recent regression-based methods [21, 25] in terms of root-relative 3D pose estimation while allowing the acquisition of absolute location information, which the other methods are incapable of.

5.4. Cascading with 2D pose estimator

In this subsection, we present the performance of the proposed cascade approach with a 2D pose estimator in estimating 3D human pose from a single RGB image. Ta-

Input 2D pose	Loc.&Scale	MPJPE	PA-MPJPE	MRPE
GT		64.97	45.47	680.38
GT	✓	61.53	45.45	239.35
2D estimate	✓	58.90	43.54	209.44
Single Gaussian	✓	56.01	44.78	164.51
Mixture model	✓	53.14	42.63	144.24

Table 2: The results of our cascade approach are presented along the input generating strategy for AbsPoseLifter learning. The Human3.6M dataset is used. “Loc.&Scale” indicates that the 2D location and scale information is utilized in AbsPoseLifter. “2D estimate” means to use the output of the 2D pose estimator as a training set. “Single Gaussian” and “Mixture model” represent the error model used for synthesizing the 2D pose.

ble 2 provides the results for the Human3.6M dataset. As with 2D-to-3D pose lifting, the approximate 2D location and scale information of the target subject boosts the performance of the root-relative pose and the absolute root location, which are evaluated through MPJPE and MRPE, respectively.

Synthesizing 2D pose for AbsPoseLifter. As shown in Table 2, the input 2D pose data used for AbsPoseLifter learning play an important role in the performance of 3D pose estimation. First, the use of ground truth 2D pose provides the worst results. This result is improved by using real 2D pose estimates obtained by applying the 2D pose estimator to training images for AbsPoseLifter learning. Evidently, the use of realistic input data for learning helps improve the performance of the model. However, such input data are fixed for a given specific training data, thereby limiting their variability. One approach to overcome this problem is to synthesize the input data in accordance with the underlying distribution. The experiment that uses the error model obtained by analyzing the actual 2D pose error statistics demonstrates that the single Gaussian model does not lead to substantial performance improvement. Figure 5 shows that the single Gaussian model estimates a larger standard deviation than necessary because of outliers. By contrast, our proposed mixture model yields considerably improved results for all the evaluation metrics. The results clearly prove our hypothesis that the synthesis of realistic inputs is beneficial for the performance of the model.

Root location estimation. To estimate the root’s absolute location, our learning-based method relies on a large-scale 2D/3D pose dataset. In [22], a method was proposed for analytically calculating the root position from given 2D and root-relative 3D poses without learning. This method assumes a weak perspective projection and is based on a linear least squares formulation. Refer to the supplementary material of [22] for the formula for calculating the depth Z

Method	MRPE	MRPE-X	MRPE-Y	MRPE-Z
Mehta [22]	163.96	20.42	20.23	157.53
Ours	144.24	20.35	20.97	137.03

Table 3: Quantitative results of root location estimation are given for the method in [22] and ours, in which the Human3.6M dataset is used. MRPE-X, MRPE-Y, and MRPE-Z represent the mean of the errors in the X , Y , and Z axes, respectively.

of the root. The remaining X and Y coordinates are obtained using a back-projection formula. Table 3 presents a quantitative comparison between the analytic approach presented in [22] and our learning-based approach, in which 2D and 3D root-relative poses obtained through our method are used for a fair comparison. Our method exhibits a better Z error than the analytic method. For the errors in the X and Y directions, our method produces nearly the same result as the analytic method, which relies on the constraint that the 3D point should be located on the back-projecting ray. This finding shows that our pose lifting method implicitly enforces such constraints through learning.

Quantitative comparison. Table 4 provides the quantitative results of the performance of recently proposed methods for 3D human pose estimation from a single RGB image. The proposed method achieves comparable performance with state-of-the-art methods for Protocols 1 and 2. In particular, our method outperforms all cascade approaches [3, 8, 21, 25, 30] that consist of a sequential combination of a 2D pose estimator and a 3D lifter. Two direct methods in [36] and [42] yield better results than ours for Protocols 1 and 2, respectively. However, several methods [36, 42, 43], including the two aforementioned methods, require the ground truth for the absolute depth of the root joint to produce a 3D pose result. This constraint is attributed to these methods using a back-projection formula to transform the joint’s estimated image coordinates x and y to 3D coordinates X and Y , wherein the absolute depth of each joint is required. By contrast, our method exhibits the advantage of not requiring ground truth because it estimates the absolute location of the root. The qualitative results for some of the images in the test dataset are shown in Figure 7.

MPI-INF-3DHP. Subsequently, we present the evaluation results of the proposed method for the MPI-INF-3DHP dataset, as shown in Table 5. We use an additional 2D pose dataset, *i.e.*, MPII, to learn the 2D pose estimator following [22]. AbsPoseLifter is learned using either the Human3.6M or the MPI-INF-3DHP, and the input synthesis method presented in Section 4.2 is applied to this process.

In contrast with the Human3.6M dataset, the focal length parameters of the cameras used to acquire the training and test sets for the MPI-INF-3DHP dataset are considerably

Protocol 1	Direct.	Discuss	Eating	Greet	Phone	Pose	Purch.	Sit	SitD.	Smoke	Photo	Wait	Walk	WalkD.	WalkT.	Avg.	GT
<i>Direct approaches</i>																	
Kanazawa CVPR'18 [16]	-	-	-	-	-	-	-	-	-	-	-	-	-	-	-	88.0	
Mehta 3DV'17 [22]	57.5	68.6	59.6	67.3	78.1	56.9	69.1	98.0	117.5	69.5	82.4	68.0	55.3	76.5	61.4	72.9	
Pavlakos CVPR'17 [29]	67.4	72.0	66.7	69.1	72.0	65.0	68.3	83.7	96.5	71.7	77.0	65.8	59.1	74.9	63.2	71.9	
Sárándi ECCVW'18 [33]	63.6	65.5	56.0	62.1	64.0	60.7	64.8	76.7	93.0	63.3	69.7	62.0	68.8	61.3	54.1	65.7	
Zhou ICCV'17 [43]	54.8	60.7	58.2	71.4	62.0	53.8	55.6	75.2	111.6	64.1	65.5	66.0	63.2	51.4	55.3	64.9	
Sun ICCV'17 [35]	52.8	54.8	54.2	54.3	61.8	53.1	53.6	71.7	86.7	61.5	67.2	53.4	47.1	61.6	53.4	59.1	
Yang CVPR'18 [42]	51.5	58.9	50.4	57.1	62.1	49.8	52.7	69.2	85.2	57.4	65.4	58.4	60.1	43.6	47.7	58.6	
Sárándi ECCVW'18 [33]*	49.1	54.6	50.4	50.7	54.8	47.4	50.1	67.5	78.4	53.1	57.4	50.7	54.0	46.1	40.1	54.2	
Sun ECCV'18 [36]	47.5	47.7	49.5	50.2	51.4	43.8	46.4	58.9	65.7	49.4	55.8	47.8	38.9	49.0	43.8	49.6	
<i>Cascade approaches</i>																	
Zhou TPAMI'18 [46]	68.7	74.8	67.8	76.4	76.3	84.0	70.2	88.0	113.8	78.0	98.4	90.1	62.6	75.1	73.6	79.9	
Martinez ICCV'17 [21]	51.8	56.2	58.1	59.0	69.5	55.2	58.1	74.0	94.6	62.3	78.4	59.1	49.5	65.1	52.4	62.9	
Fang AAAI'18 [8]	50.1	54.3	57.0	57.1	66.6	53.4	55.7	72.8	88.6	60.3	73.3	57.7	47.5	62.7	50.6	60.4	
Ours	44.8	48.2	48.5	51.1	54.5	47.9	47.8	60.7	76.4	52.5	64.4	50.8	39.0	55.3	42.2	52.5	
Protocol 2	Direct.	Discuss	Eating	Greet	Phone	Pose	Purch.	Sit	SitD.	Smoke	Photo	Wait	Walk	WalkD.	WalkT.	Avg.	GT
<i>Direct approaches</i>																	
Kanazawa CVPR'18 [16]	-	-	-	-	-	-	-	-	-	-	-	-	-	-	-	56.8	
Sun ECCV'18 [36]	36.9	36.2	40.6	40.4	41.9	34.9	35.7	50.1	59.4	40.4	44.9	39.0	30.8	39.8	36.7	40.6	
Yang CVPR'18 [42]	26.9	30.9	36.3	39.9	43.9	28.8	29.4	36.9	58.4	41.5	47.4	30.5	42.5	29.5	32.2	37.7	
<i>Cascade approaches</i>																	
Ramakrishna ECCV'12 [30]	137.4	149.3	141.6	154.3	157.7	141.8	158.1	168.6	175.6	160.4	158.9	161.7	174.8	150.0	150.2	157.3	
Bogo ECCV'16 [3]	62.0	60.2	67.8	76.5	92.1	73.0	75.3	100.3	137.3	83.4	77.0	77.3	79.7	86.8	87.7	82.3	
Moreno-Noguer CVPR'17 [25]	66.1	61.7	84.5	73.7	65.2	60.9	67.3	103.5	74.6	92.6	67.2	69.6	78.0	71.5	73.2	74.0	
Zhou TPAMI'18 [46]	47.9	48.8	52.7	55.0	56.8	49.0	45.5	60.8	81.1	53.7	65.5	51.6	50.4	54.8	55.9	55.3	
Martinez ICCV'17 [21]	39.5	43.2	46.4	47.0	51.0	41.4	40.6	56.5	69.4	49.2	56.0	45.0	38.0	49.5	43.1	47.7	
Fang AAAI'18 [8]	38.2	41.7	43.7	44.9	48.5	40.2	38.2	54.5	64.4	47.2	55.3	44.3	36.7	47.3	41.7	45.7	
Ours	32.7	36.0	45.1	38.3	37.2	36.3	32.4	36.7	58.4	41.2	46.2	36.2	27.2	47.3	32.5	39.1	

Table 4: A quantitative comparison of our approach and other recent methods for 3D human pose estimation from a single RGB image is illustrated. “*” indicates additional Pascal VOC dataset [7] is used for training. “GT” means that the root’s ground truth depth has been used during the estimation process. The Human3.6M dataset is used. MPJPE and PA-MPJPE are adopted for Protocols 1 and 2, respectively.

Method	3D Dataset	StudioGS	StudioNoGS	Outdoor	All 3DPCK	AUC	MRPE
Yang [42]	H3.6M	-	-	-	69.0	32.0	-
Zhou [43]	H3.6M	71.1	64.7	72.7	69.2	32.5	-
Ours w/o canonical loss	H3.6M	81.1	73.5	72.5	76.2	40.0	920.1
Ours	H3.6M	81.6	73.6	72.5	76.5	40.2	421.3
Mehta [22]	INF	84.1	68.9	59.6	72.5	36.9	-
Mehta [22]	INF+H3.6M	84.6	72.4	69.7	76.5	40.8	-
Mehta [23]	INF+H3.6M	-	-	-	76.6	40.4	-
Kanazawa [16]	INF+H3.6M	-	-	-	72.9	36.5	-
Ours w/o canonical loss	INF	91.4	83.0	74.1	84.0	45.1	260.8
Ours	INF	91.4	82.9	73.7	83.9	45.0	217.4

Table 5: The comparison results of the proposed and other methods are shown for the MPI-INF-3DHP dataset. “Ours w/o canonical loss” means that the canonical loss function is not used.

different. By the focal length ambiguity, this allows a single input 2D pose to be mapped to multiple absolute root depths corresponding to different focal length parameters. Therefore, learning to regress the absolute root depth directly, based on a dataset containing different focal length images, becomes a seriously ill-posed problem. The *canonical loss function* proposed in Section 3.2 resolves this problem by causing our network to regress the canonical root depth normalized by the focal length, as shown in Table 5. We can see that the use of the canonical loss function results in a significantly reduced MRPE.

Table 5 also presents the quantitative comparison be-

tween the proposed approach and the existing state-of-the-art methods. For the experiments using the Human3.6M dataset, our method performs better than recent state-of-the-art methods that are based on a geometric constraint [43] and adversarial learning [42]. This finding shows that the proposed model can be generalized to unseen test data not used for learning. When the MPI-INF-3DHP dataset is used for learning, the proposed method outperforms all the other approaches. Figure 8 shows the qualitative results for some test images.

Qualitative results for in-the-wild images. We apply the proposed method to the in-the-wild images of the COCO

dataset [19]. To detect bounding boxes that contain persons from an input image, we use Mask R-CNN [10] that is pre-trained from the COCO dataset. Then we estimate the absolute 3D pose by feeding the image and detected bounding boxes to our cascade model. The focal length is manually selected. Figure 9 shows the estimated 3D poses. We can see that the proposed method can be used in conjunction with the object detector to perform 3D pose estimation on challenging in-the-wild images successfully.

6. Conclusion

In this study, we propose a novel pose lifting method (*i.e.*, AbsPoseLifter) for estimating a 3D human pose from a 2D human pose. In contrast with previous methods, the proposed method enables the acquisition of an absolute pose (*i.e.*, a root-relative pose with absolute root coordinates) in a camera coordinate system and achieves the state-of-the-art pose lifting performance. We also propose a simple cascade approach, namely, a sequential combination of a 2D pose estimator and AbsPoseLifter, for 3D human pose estimation from a single RGB image. In this case, utilizing the error statistics of 2D pose estimation for AbsPoseLifter learning is essential and contributes to the state-of-the-art 3D pose estimation performance of the proposed approach.

References

- [1] I. Akhter and M. J. Black. Pose-conditioned joint angle limits for 3d human pose reconstruction. In *Proc. IEEE Conf. Computer Vision and Pattern Recognition (CVPR)*, pages 1446–1455, 2015. 3
- [2] M. Andriluka, L. Pishchulin, P. Gehler, and B. Schiele. 2d human pose estimation: New benchmark and state of the art analysis. In *Proc. IEEE Conf. Computer Vision and Pattern Recognition (CVPR)*, pages 3686–3693, 2014. 7
- [3] F. Bogo, A. Kanazawa, C. Lassner, P. Gehler, J. Romero, and M. J. Black. Keep it smpl: Automatic estimation of 3d human pose and shape from a single image. In *Proc. European Conf. Computer Vision (ECCV)*, pages 561–578, 2016. 3, 9, 10
- [4] J. Y. Chang. Nonparametric feature matching based conditional random fields for gesture recognition from multimodal video. *IEEE Trans. Pattern Analysis and Machine Intelligence*, 38(8):1612–1625, 2016. 1
- [5] Y. Dai, H. Li, and M. He. A simple prior-free method for non-rigid structure-from-motion factorization. *International Journal of Computer Vision*, 107(2):101–122, 2014. 8
- [6] A. P. Dempster, N. M. Laird, and D. B. Rubin. Maximum likelihood from incomplete data via the em algorithm. *Journal of the Royal Statistical Society: Series B (Methodological)*, 39(1):1–22, 1977. 6
- [7] M. Everingham, L. Van Gool, C. K. Williams, J. Winn, and A. Zisserman. The pascal visual object classes (voc) challenge. *International Journal of Computer Vision*, 88(2):303–338, 2010. 10
- [8] H.-S. Fang, Y. Xu, W. Wang, X. Liu, and S.-C. Zhu. Learning pose grammar to encode human body configuration for 3d pose estimation. In *AAAI Conference on Artificial Intelligence*, 2018. 3, 9, 10
- [9] J. C. Gower. Generalized procrustes analysis. *Psychometrika*, 40(1):33–51, 1975. 7
- [10] K. He, G. Gkioxari, P. Dollár, and R. Girshick. Mask r-cnn. In *Proc. IEEE Int'l Conf. Computer Vision (ICCV)*, pages 2961–2969, 2017. 11
- [11] K. He, X. Zhang, S. Ren, and J. Sun. Deep residual learning for image recognition. In *Proc. IEEE Conf. Computer Vision and Pattern Recognition (CVPR)*, pages 770–778, 2016. 5, 6
- [12] S. Ioffe and C. Szegedy. Batch normalization: Accelerating deep network training by reducing internal covariate shift. In *Proc. International Conference on Machine Learning*, 2015. 5
- [13] C. Ionescu, D. Papava, V. Olaru, and C. Sminchisescu. Human3.6m: Large scale datasets and predictive methods for 3d human sensing in natural environments. *IEEE Trans. Pattern Analysis and Machine Intelligence*, 36(7):1325–1339, 2014. 3, 7
- [14] H. Jhuang, J. Gall, S. Zuffi, C. Schmid, and M. J. Black. Towards understanding action recognition. In *Proc. IEEE Int'l Conf. Computer Vision (ICCV)*, pages 3192–3199, 2013. 1
- [15] G. Johansson. Visual motion perception. *Scientific American*, 1975. 1
- [16] A. Kanazawa, M. J. Black, D. W. Jacobs, and J. Malik. End-to-end recovery of human shape and pose. In *Proc. IEEE Conf. Computer Vision and Pattern Recognition (CVPR)*, pages 7122–7131, 2018. 10
- [17] H.-J. Lee and Z. Chen. Determination of 3d human body postures from a single view. *Computer Vision, Graphics, and Image Processing*, 30(2):148–168, 1985. 1
- [18] S. Li and A. B. Chan. 3d human pose estimation from monocular images with deep convolutional neural network. In *Proc. Asian Conference on Computer Vision (ACCV)*, pages 332–347, 2014. 3
- [19] T.-Y. Lin, M. Maire, S. Belongie, J. Hays, P. Perona, D. Ramanan, P. Dollár, and C. L. Zitnick. Microsoft coco: Common objects in context. In *Proc. European Conf. Computer Vision (ECCV)*, pages 740–755, 2014. 11
- [20] D. C. Luvizon, H. Tabia, and D. Picard. Human pose regression by combining indirect part detection and contextual information. *arXiv preprint arXiv:1710.02322*, 2017. 3
- [21] J. Martinez, R. Hossain, J. Romero, and J. J. Little. A simple yet effective baseline for 3d human pose estimation. In *Proc. IEEE Int'l Conf. Computer Vision (ICCV)*, pages 2640–2649, 2017. 1, 3, 4, 5, 8, 9, 10
- [22] D. Mehta, H. Rhodin, D. Casas, P. Fua, O. Sotnychenko, W. Xu, and C. Theobalt. Monocular 3d human pose estimation in the wild using improved cnn supervision. In *International Conference on 3D Vision (3DV)*, pages 506–516, 2017. 3, 7, 9, 10
- [23] D. Mehta, S. Sridhar, O. Sotnychenko, H. Rhodin, M. Shafei, H.-P. Seidel, W. Xu, D. Casas, and C. Theobalt. Vnect: Real-time 3d human pose estimation with a single rgb camera. *ACM Transactions on Graphics (TOG)*, 36(4), 2017. 10

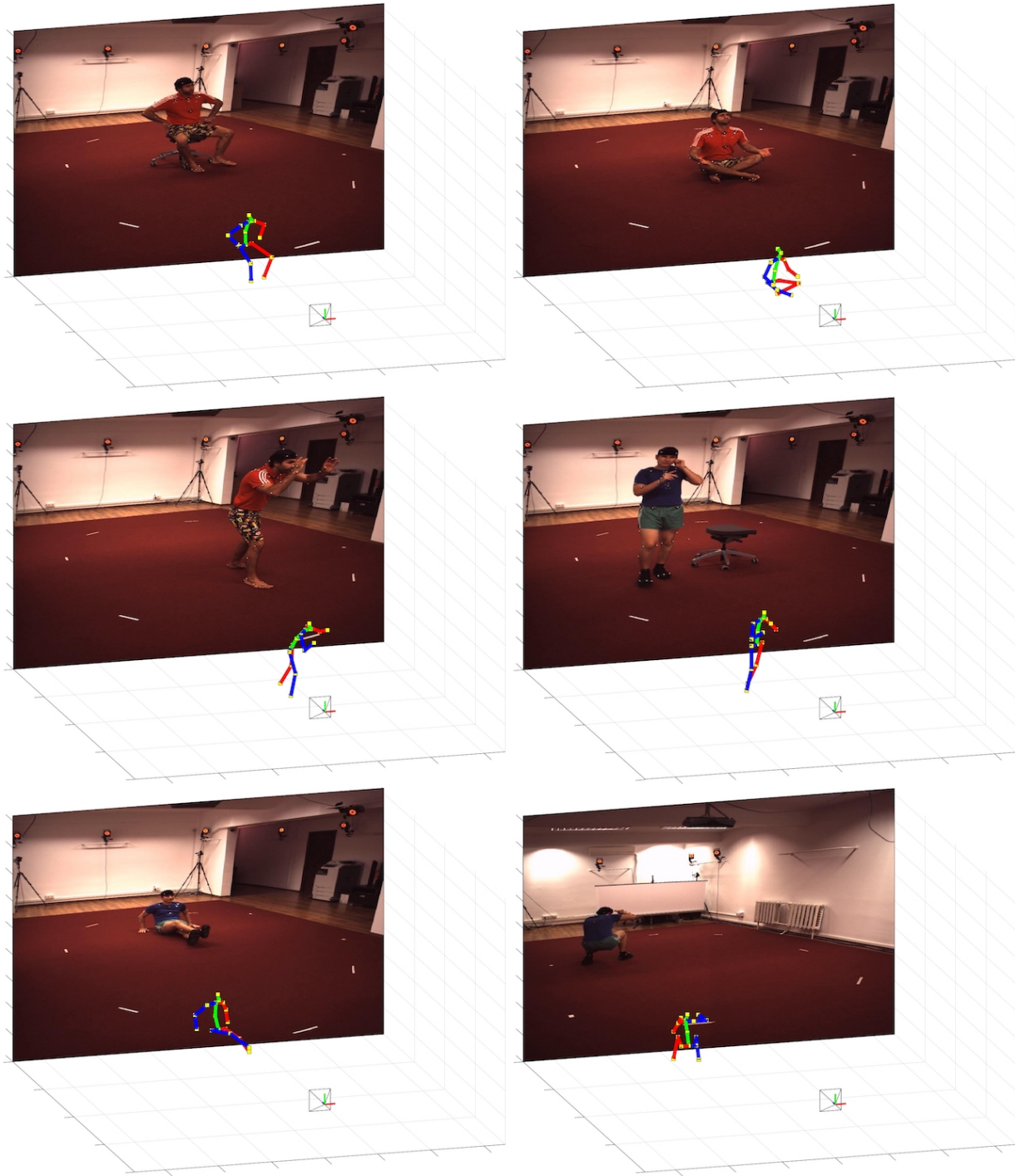


Figure 7: Qualitative results of our method are shown for the Human3.6M dataset.

- [24] G. Moon, J. Y. Chang, and K. M. Lee. Posefix: Model-agnostic general human pose refinement network. In *Proc. IEEE Conf. Computer Vision and Pattern Recognition (CVPR)*, 2019. [2](#), [3](#)
- [25] F. Moreno-Noguer. 3d human pose estimation from a single image via distance matrix regression. In *Proc. IEEE Conf. Computer Vision and Pattern Recognition (CVPR)*, pages 2823–2832, 2017. [3](#), [8](#), [9](#), [10](#)
- [26] V. Nair and G. E. Hinton. Rectified linear units improve restricted boltzmann machines. In *Proc. International Conference on Machine Learning*, pages 807–814, 2010. [5](#)
- [27] A. Nibali, Z. He, S. Morgan, and L. Prendergast. Numerical

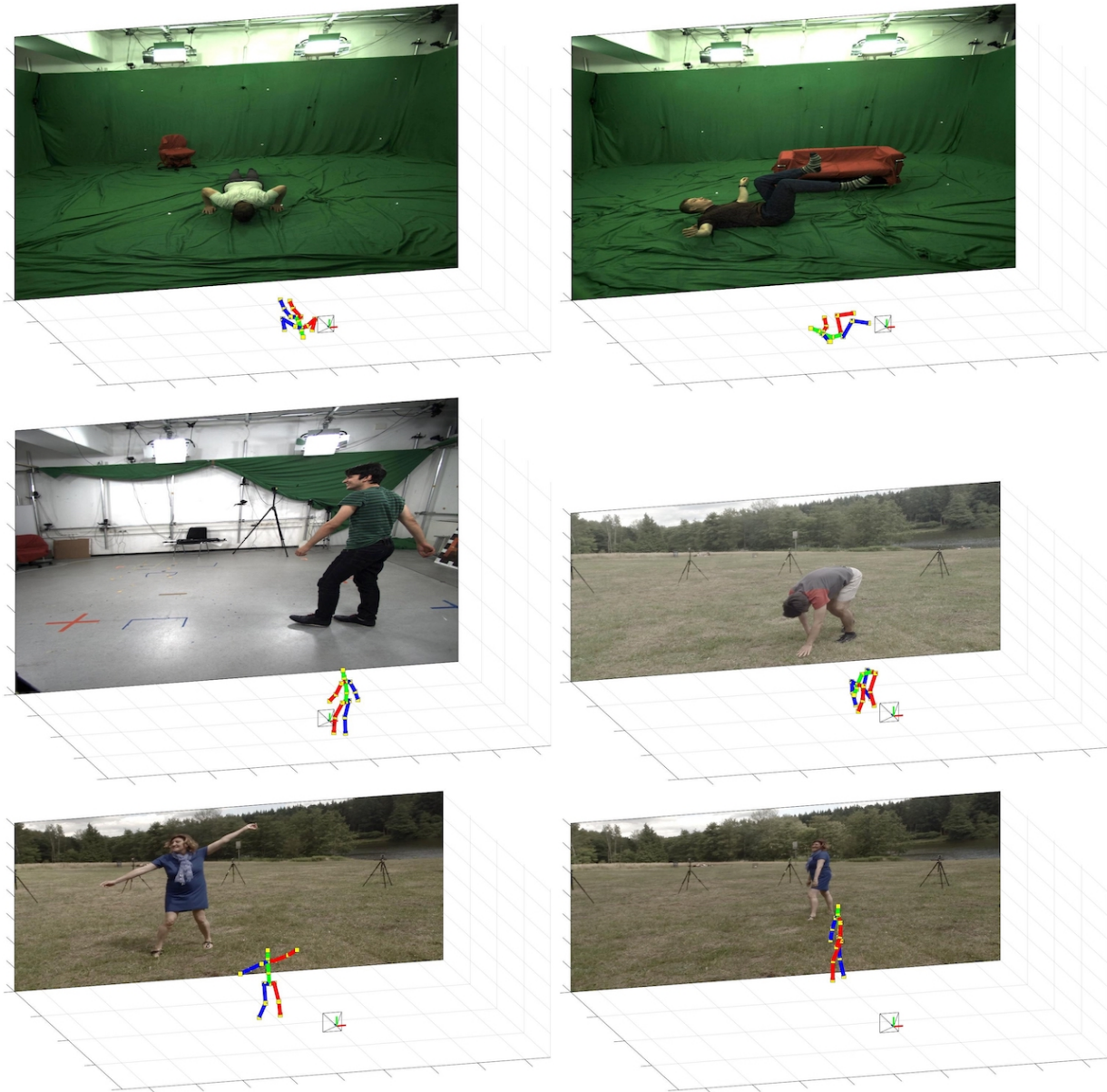


Figure 8: Qualitative results of our method are shown for the MPI-INF-3DHP dataset.

coordinate regression with convolutional neural networks.
arXiv preprint arXiv:1801.07372, 2018. 3

- [28] A. Paszke, S. Gross, S. Chintala, G. Chanan, E. Yang, Z. DeVito, Z. Lin, A. Desmaison, L. Antiga, and A. Lerer. Automatic differentiation in pytorch. In *Advances in Neural Information Processing Systems Workshops*, 2017. 7
- [29] G. Pavlakos, X. Zhou, K. G. Derpanis, and K. Daniilidis. Coarse-to-fine volumetric prediction for single-image 3d human pose. In *Proc. IEEE Conf. Computer Vision and Pattern Recognition (CVPR)*, pages 7025–7034, 2017. 3, 10
- [30] V. Ramakrishna, T. Kanade, and Y. Sheikh. Reconstructing 3d human pose from 2d image landmarks. In *Proc. European Conf. Computer Vision (ECCV)*, pages 573–586, 2012. 1, 3

8, 9, 10

- [31] M. R. Ronchi and P. Perona. Benchmarking and error diagnosis in multi-instance pose estimation. In *Proc. IEEE Int'l Conf. Computer Vision (ICCV)*, pages 369–378, 2017. 2, 3, 6
- [32] O. Russakovsky, J. Deng, H. Su, J. Krause, S. Satheesh, S. Ma, Z. Huang, A. Karpathy, A. Khosla, M. Bernstein, A. C. Berg, and L. Fei-Fei. Imagenet large scale visual recognition challenge. *International Journal of Computer Vision*, 115(3):211–252, 2015. 7
- [33] I. Sárándi, T. Linder, K. O. Arras, and B. Leibe. Synthetic occlusion augmentation with volumetric heatmaps for the 2018 eccv posetrack challenge on 3d human pose estimation.

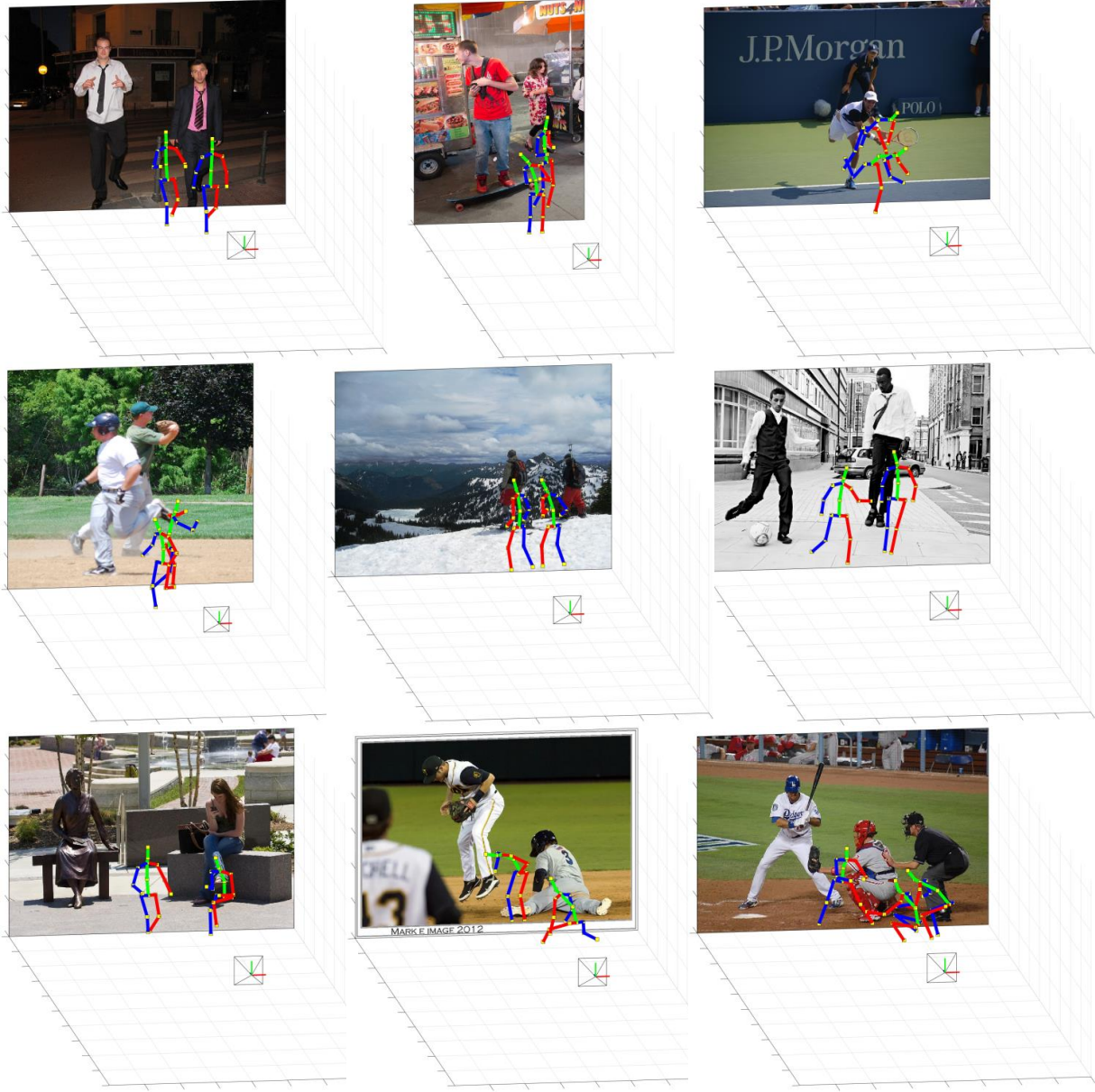


Figure 9: Qualitative results of our method are shown for the in-the-wild images of the COCO dataset.

arXiv preprint arXiv:1809.04987, 2018. 3, 10

- [34] N. Srivastava, G. Hinton, A. Krizhevsky, I. Sutskever, and R. Salakhutdinov. Dropout: a simple way to prevent neural networks from overfitting. *Journal of Machine Learning Research*, 15(1):1929–1958, 2014. 5
- [35] X. Sun, J. Shang, S. Liang, and Y. Wei. Compositional human pose regression. In *Proc. IEEE Int'l Conf. Computer Vision (ICCV)*, pages 2602–2611, 2017. 3, 10
- [36] X. Sun, B. Xiao, F. Wei, S. Liang, , and Y. Wei. Integral human pose regression. In *Proc. European Conf. Computer Vision (ECCV)*, 2018. 3, 6, 9, 10
- [37] T. Tieleman and G. Hinton. Lecture 6.5-rmsprop: Divide the gradient by a running average of its recent magnitude. *COURSERA: Neural Networks for Machine Learning*, 2012. 7
- [38] J. J. Tompson, A. Jain, Y. LeCun, and C. Bregler. Joint training of a convolutional network and a graphical model for human pose estimation. In *Advances in Neural Information Processing Systems*, pages 1799–1807, 2014. 8
- [39] A. Toshev and C. Szegedy. Deeppose: Human pose estimation via deep neural networks. In *Proc. IEEE Conf. Computer Vision and Pattern Recognition (CVPR)*, pages 1653–1660, 2014. 8
- [40] C. Wang, Y. Wang, Z. Lin, A. L. Yuille, and W. Gao. Ro-

bust estimation of 3d human poses from a single image. In *Proc. IEEE Conf. Computer Vision and Pattern Recognition (CVPR)*, pages 2361–2368, 2014. 3

[41] B. Xiao, H. Wu, and Y. Wei. Simple baselines for human pose estimation and tracking. In *Proc. European Conf. Computer Vision (ECCV)*, pages 466–481, 2018. 6

[42] W. Yang, W. Ouyang, X. Wang, J. Ren, H. Li, and X. Wang. 3d human pose estimation in the wild by adversarial learning. In *Proc. IEEE Conf. Computer Vision and Pattern Recognition (CVPR)*, pages 5255–5264, 2018. 9, 10

[43] X. Zhou, Q. Huang, X. Sun, X. Xue, and Y. Wei. Towards 3d human pose estimation in the wild: A weakly-supervised approach. In *Proc. IEEE Int'l Conf. Computer Vision (ICCV)*, 2017. 9, 10

[44] X. Zhou, S. Leonardos, X. Hu, and K. Daniilidis. 3d shape estimation from 2d landmarks: A convex relaxation approach. In *Proc. IEEE Conf. Computer Vision and Pattern Recognition (CVPR)*, pages 4447–4455, 2015. 3, 8

[45] X. Zhou, M. Zhu, S. Leonardos, K. Derpanis, and K. Daniilidis. Sparseness meets deepness: 3d human pose estimation from monocular video. In *Proc. IEEE Conf. Computer Vision and Pattern Recognition (CVPR)*, 2016. 8

[46] X. Zhou, M. Zhu, G. Pavlakos, S. Leonardos, K. G. Derpanis, and K. Daniilidis. Monocap: Monocular human motion capture using a cnn coupled with a geometric prior. *IEEE Trans. Pattern Analysis and Machine Intelligence*, 41(4):901–914, 2018. 10